STOCHASTICALLY GENERATED MULTIGROUP DIFFUSION COEFFICIENTS

A Thesis
Presented to
The Academic Faculty

by

Justin M. Pounders

In Partial Fulfillment
of the Requirements for the Degree
Master of Science in Nuclear Engineering

Georgia Institute of Technology
December 2006

STOCHASTICALLY GENERATED MULTIGROUP DIFFUSION COEFFICIENTS

Approved by:

Dr. Farzad Rahnema, Advisor
School of Mechanical Engineering
Georgia Institute of Technology

Dr. Weston Stacey
School of Mechanical Engineering
Georgia Institute of Technology

Dr. Nolan Hertel
School of Mechanical Engineering
Georgia Institute of Technology

Date Approved: 20 November 2006

ACKNOWLEDGEMENTS

I would first like to thank my advisor, Dr. Rahnema, for his guidance, instruction and support over the past several years. His direction and insight have been invaluable.

Words can not express my appreciation for my wife, Sarah, for her continual love, support and encouragement in all areas of my life, graduate school being only one of them. I am also blessed to have had the life-long support of my parents, Randy and Lynda Pounders.

The research for this thesis was performed under appointment to the Naval Nuclear Propulsion Fellowship Program sponsored by the Naval Reactors Division of the United States Department of Energy.

TABLE OF CONTENTS

LIST OF TABLES

LIST OF FIGURES

SUMMARY

The generation of multigroup neutron cross sections is usually the first step in the solution of reactor physics problems. This typically includes generating condensed cross section sets, collapsing the scattering kernel, and within the context of diffusion theory, computing diffusion coefficients that capture transport effects as accurately possible. Although the calculation of multigroup parameters has historically been done via deterministic methods, it is natural to think of using the Monte Carlo method due to its geometric flexibility and robust computational capabilities such as continuous energy transport.

For this reason, a stochastic cross section generation method has been implemented in the Mont Carlo code MCNP5 (Brown et al, 2003) that is capable of computing macroscopic material cross sections (including angular expansions of the scattering kernel) for transport or diffusion applications. This methodology includes the capability of tallying arbitrary-order Legendre expansions of the scattering kernel. Furthermore, several approximations of the diffusion coefficient have been developed and implemented. The accuracy of these stochastic diffusion coefficients within the multigroup framework is investigated by examining a series of simple reactor problems.

CHAPTER 1

INTRODUCTION

The ultimate goal of steady-state reactor physics calculations is to determine the distribution of neutrons in space, angle and energy within a reactor so that key integral quantities such as the power distribution and the neutron multiplication rate can be evaluated. Since solving the Boltzmann transport equation continuously in all variables is computationally prohibitive, certain simplifying assumptions must be made.

The most common simplification of the transport equation is the multigroup method, where the energy domain is divided into a finite number of contiguous sub-intervals. A great deal of care must be given to collapsing the continuous energy transport equation, however, to ensure that the multigroup equations are generated in a consistent manner capable of reproducing the true solution with as little approximation as possible. The calculation of multigroup parameters is key to the solution of reactor physics problems.

The treatment of the angular dependence of the transport equation, on the other hand, is usually what differentiates one transport approximation from another, giving rise to diffusion theory, the P_N method, the discrete ordinates method, etc. Of all these approximations, diffusion theory is unique in that it does not explicitly treat the angular dependence. Instead, the angular dependence of the problem is wrapped into a single parameter—the diffusion coefficient. This feature makes the transport problem much easier to solve, but often sacrifices accuracy in the process. The calculation of diffusion coefficients, however, is not as clearly defined as other multigroup parameters. It is usually the case that diffusion coefficients are born out of approximations whose validity largely depends on the type of problem at hand.

Due to constraints in computing power, the calculations of these multigroup parameters (and reactor physics problems in general) have normally been carried out via deterministic methods. As computer technology has advanced however, stochastic methods have been employed more frequently to generate high-accuracy solutions to transport problems. The geometric flexibility and lack of approximation associated with the Monte Carlo method makes it very suitable for the generation of highly accurate multigroup cross sections and high-order diffusion coefficients, although it has not historically been used for such applications.

This thesis will therefore analyze several definitions of the diffusion coefficient within the framework of stochastic cross section generation. The goal is to compute diffusion coefficients that maximize the accuracy of traditional fine mesh diffusion methods. The next chapter reviews a methodology for computing general multigroup parameters within Monte Carlo methods. Subsequently several diffusion coefficients are derived and their implementation in a Monte Carlo setting discussed. Finally, some numerical results are shown and some final conclusions drawn.

CHAPTER 2

BACKGROUND

The goal of many reactor physics problem is solving the time-independent neutron transport equation which can be written

$$\hat{\Omega}\cdot\nabla\psi(\mathbf{r},E,\hat{\Omega})+\sigma(\mathbf{r},E)\psi(\mathbf{r},E,\hat{\Omega})= \int dE'\int_{4\pi}d\hat{\Omega}'\left[\sigma_s(\mathbf{r},E'\to E,\mu_0)+\chi(E)\nu(E')\sigma_f(\mathbf{r},E')\right]\psi(\mathbf{r},E',\hat{\Omega}') \quad (1)$$

where ψ is the angular flux density, σ is the macroscopic neutron cross section, and χ and ν are the fission spectrum and yield, respectively, and μ_0 is the scattering angle between $\hat{\Omega}$ and $\hat{\Omega}'$. The phase space has been defined in terms of the neutron position, energy and direction of flight. Out of convenience, it has been assumed that there is no external source.

Deterministic transport methods usually treat the scattering cross section of Equation (1) in terms of a Legendre expansion in the scattering angle, $\mu_0=\hat{\Omega}\cdot\hat{\Omega}'$:

$$\sigma_s(\mathbf{r},E'\to E,\mu_0)=\sum_{\ell=1}^{\infty}\frac{2\ell+1}{2}\sigma_{s,\ell}(\mathbf{r},E'\to E)P_\ell(\mu_0) \quad (2)$$

where the scattering moment has been defined

$$\sigma_{s,\ell}(\mathbf{r},E'\to E)=\int_{-1}^{1}d\mu_0\sigma_s(\mathbf{r},E'\to E,\mu_0)P_\ell(\mu_0)\,. \quad (3)$$

Recalling the addition theorem for Legendre polynomials in terms of spherical harmonics, $P_\ell(\mu_0)=\sum_{m=-\ell}^{\ell}Y_{\ell m}(\hat{\Omega})Y_{\ell m}^{*}(\hat{\Omega}')$, and plugging this expansion into Equation (1) results in the following expression:

$$\hat{\Omega}\cdot\nabla\psi(\mathbf{r},E,\hat{\Omega})+\sigma(\mathbf{r},E)\psi(\mathbf{r},E,\hat{\Omega})= \int dE'\left[\sum_{\ell=0}^{\infty}\frac{2\ell+1}{2}\sigma_{s,\ell}(\mathbf{r},E'\to E)\sum_{m=-\ell}^{\ell}\psi_{\ell m}(\mathbf{r},E')Y_{\ell m}(\hat{\Omega})+.\right. \left.\chi(E)\int dE'\nu(E')\sigma_f(\mathbf{r},E')\psi(\mathbf{r},E',\hat{\Omega}')\right] \quad (4)$$

where the angular flux moment, $\psi_{\ell m}$, has been implicitly defined through the integration over angle, $\hat{\Omega}'$, with spherical harmonics.

2.1. Multigroup Formulation

The continuous energy dependence of the transport equation is rarely treated explicitly. Instead it is common to integrate the equation over contiguous energy ranges, giving rise to the multigroup expression of the transport equation:

$$\hat{\Omega}\cdot\nabla\psi_g(\mathbf{r},\hat{\Omega})+\sigma_g(\mathbf{r})\psi_g(\mathbf{r},\hat{\Omega})= \sum_{g'=1}^{G}\left[\sum_{\ell=0}^{\infty}\frac{2\ell+1}{2}\sigma_{s,\ell}^{g'g}(\mathbf{r})\sum_{m=-\ell}^{\ell}\psi_{\ell m,g'}(\mathbf{r})Y_{\ell m}(\hat{\Omega})+\chi_g\nu\sigma_{f,g'}(\mathbf{r})\varphi_{g'}(\mathbf{r})\right] \quad (5)$$

where there is a total of *G* energy groups. The fission emission is assumed to be isotropic which enables the fission term to be written in terms of the scalar flux, $\varphi(\mathbf{r},E)=\int_{4\pi}\psi(\mathbf{r},E,\hat{\Omega})$.

Comparing the terms of Equations (4) and (5) gives rise to the following definitions of the multigroup constants:

$$\psi_g(\mathbf{r},\hat{\Omega}) = \int_{E_{g+1}}^{E_g} dE'\psi(\mathbf{r},E',\hat{\Omega})$$

$$\sigma_g(\mathbf{r},\hat{\Omega}) = \frac{\int_{E_{g+1}}^{E_g} dE'\sigma(\mathbf{r},E')\psi(\mathbf{r},E',\hat{\Omega})}{\int_{E_{g+1}}^{E_g} dE'\psi(\mathbf{r},E',\hat{\Omega})}$$

$$\nu\sigma_{f,g}(\mathbf{r}) = \frac{\int_{E_{g+1}}^{E_g} dE'\nu(E')\sigma_f(\mathbf{r},E')\varphi(\mathbf{r},E')}{\int_{E_{g+1}}^{E_g} dE'\varphi(\mathbf{r},E')} \tag{6}$$

$$\sigma_{s,\ell}^{g'g}(\mathbf{r},\hat{\Omega}) = \frac{\int_{E_{g+1}}^{E_g} dE\int_{E_{g'+1}}^{E_{g'}} dE'\sigma_{s,\ell}(\mathbf{r},E'\to E)\sum_{m=-\ell}^{\ell}\psi_{\ell m}(\mathbf{r},E')Y_{\ell m}(\hat{\Omega})}{\int_{E_{g+1}}^{E_g} dE'\sum_{m=-\ell}^{\ell}\psi_{\ell m}(\mathbf{r},E')Y_{\ell m}(\hat{\Omega})}$$

where the fission yield and cross section have been treated as a single term.

The total and scattering cross sections now have an undesirable angular dependence that most transport methodologies do not accommodate. It is common practice to weight the total cross sections with the scalar flux instead. Doing so makes the assumption that the angular and energetic dependencies of the flux can be separated within a group, i.e. $\psi(\mathbf{r},E,\hat{\Omega}) = \varphi(\mathbf{r},E)f(\mathbf{r},\hat{\Omega})$, where $\int_{4\pi} d\hat{\Omega}' f(\mathbf{r},\hat{\Omega}) = 1$, thereby causing the angular dependence in the numerator and denominator to cancel. Experience has shown that using this assumption within reactor contexts to generate multigroup constants leads to accurate results as long as spatial homogenization is not used. The common definition of the total cross section, and the one which will be used presently, is therefore

$$\sigma_g(\mathbf{r}) = \frac{\int_{E_{g+1}}^{E_g} dE'\sigma(\mathbf{r},E')\varphi(\mathbf{r},E')}{\int_{E_{g+1}}^{E_g} dE'\varphi(\mathbf{r},E')}. \tag{7}$$

Similarly, the condensed scattering kernel will be defined as

$$\sigma_{s,\ell}^{g'g}(\mathbf{r}) = \frac{\int_{E_{g+1}}^{E_g} dE\int_{E_{g'+1}}^{E_{g'}} dE'\sigma_{s,\ell}(\mathbf{r},E'\to E)\varphi(\mathbf{r},E')}{\int_{E_{g+1}}^{E_g} dE'\varphi(\mathbf{r},E')}. \tag{8}$$

It is immediately evident from their definitions that the multigroup parameters can not be computed without knowledge of the continuous-energy neutron spectrum. Since this is usually not known *a priori*, most current cross section generation methods either substitute a weighting function that has approximately the same spectral shape as the neutron flux or use a fine-group or continuous energy transport method to compute an accurate flux solution, often with approximate boundary conditions or simplified geometry. The former option is limited by the approximations used to generate the weighting function. Since the validity of these approximations can vary greatly depending on their application, this option will not currently be considered any further.

The second approach is limited by the computational constraints of the transport method used to collapse the cross sections. Most deterministic transport methods, for example, are limited to one or two spatial dimensions and are incapable of utilizing continuous energy cross section libraries. Stochastic methods such as Monte Carlo, however, do not have these limitations. It is therefore natural to think of using such methods to generate multigroup cross sections.

2.2. Stochastic Cross Section Generation

A methodology for stochastically computing multigroup cross sections based on track-length estimates of neutron reaction rates was proposed by Redmond (1990). This methodology recognizes that the multigroup cross sections for 'direct' reactions (i.e. capture, fission, total, etc.) are simply the reaction rate density divided by the group flux. The reaction rate density for reaction x can be computed by the Monte Carlo tally (Briesmeister, 2000)

$$R_{x,g} = \frac{1}{NV} \sum_n \sum_i \left[\sigma_x(E_i) w_i T_i \right], \quad \text{for } E_{g+1} < E_i < E_g . \tag{9}$$

where E_i, w_i and T_i are the energy, weight and path length of track i of particle n; N is the total number of particles recorded and V is the volume of the cell associated with this tally. Likewise the scalar neutron flux tally has the form

$$F_{x,g} = \frac{1}{NV} \sum_n \sum_i \left[w_i T_i \right], \quad \text{for } E_{g+1} < E_i < E_g \,. \tag{10}$$

The collapsed cross section of type x is therefore

$$\sigma_{x,g} = \frac{R_{x,g}}{F_{x,g}} \,. \tag{11}$$

The scattering kernel requires slightly more attention since it must be tallied as a function of incoming and outgoing energies. In this case, the numerator of Equation (11) must be replaced by a tally matrix, $R_{x,g'g}$, defined by

$$R_{s,g'g} = \frac{1}{NV} \sum_n \sum_i \left[\sigma_s(E_i' \to E_i) w_i T_i \right], \quad \text{for} \begin{cases} E_{g+1} < E_i < E_g \\ E_{g'+1} < E_i' < E_{g'} \end{cases} . \tag{12}$$

Computing the Legendre moments of the scattering kernel requires only a slight modification to Equation (12). Recalling Equations (3) and (8), the collapsed scattering kernel (i.e. group-to-group scattering matrix) can be written

$$\sigma_{s,\ell}^{g'g}(\mathbf{r}) = \frac{\int_{E_{g+1}}^{E_g} dE \int_{E_{g'+1}}^{E_{g'}} dE' \int_{-1}^{1} d\mu_0 \sigma_s(\mathbf{r}, E' \to E, \mu_0) P_\ell(\mu_0) \varphi(\mathbf{r}, E')}{\int_{E_{g+1}}^{E_g} dE' \varphi(\mathbf{r}, E')} \,. \tag{13}$$

All integrations in the above expressions are performed implicitly, by virtue of the fact that the variables of integration are sampled and tallied over their entire domains through out the course of the simulation. It is therefore straightforward to see that the numerator of Equation (13) can be calculated by only a slight modification to the scattering matrix:

$$R_{s\ell,g'g} = \frac{1}{NV} \sum_n \sum_i \left[\sigma_s(E_i' \to E_i) P_\ell(\mu_i) w_i T_i \right], \quad \text{for} \begin{cases} E_{g+1} < E_i < E_g \\ E_{g'+1} < E_i' < E_{g'} \end{cases} . \tag{14}$$

It should be noted that since the preceding tallies are based on neutron track lengths, they are accrued (i.e. integrated) over a volumetric sub-region of the system, but

the analytic expressions have been written as point-wise continuous in space. To be consistent, the multigroup equation given by Equation (5) should also be integrated over the tally volume, V_T, which yields

$$\bar{\sigma}_g = \frac{\int_{V_T} dV' \int_{E_{g+1}}^{E_g} dE' \sigma(\mathbf{r}, E')\varphi(\mathbf{r}, E')}{\int_{V_T} dV' \int_{E_{g+1}}^{E_g} dE' \varphi(\mathbf{r}, E')} \tag{15}$$

where $\mathbf{r} \in V_T$. If V_T contains multiple homogenous sub-regions, then Equation (15) is a spatially homogenized cross section. Even if Equation (15) is evaluated over a spatially homogenous region, there still may be homogenization effects due to the joint variation of the flux in space and energy. Caution must therefore be exercised when collapsing cross sections to avoid unintentional homogenization.

Redmond implemented the above methodology in MCNP version 4C (Briesmeister, 2000). Modifications to the code are necessary to support the matrix tallies required for the Legendre scattering moments. Furthermore, a mechanism for sampling a scattering angle and the associated change in neutron energy at *every* tally point (whether or not the physical event occurred) was added to ensure that the cross sections were fully integrated and had reasonable statistics. The present author applied this methodology to the latest release of MCNP version 5 (Brown et al, 2003).

2.3. Transport Cross Section

One issue not addressed by Redmond is how to stochastically compute an accurate transport cross section for diffusion applications. Ilas, G. and Rahnema (2003) presented a method for tallying the transport cross section defined by

$$\sigma_{tr,g} = \sigma_g - \bar{\mu}_{0,g}\sigma_{s,g}, \tag{16}$$

where $\bar{\mu}_{0,g}$ is the average scattering angle in group g. The scattering angle was estimated by tallying the product of the incident and emergent directional cosine vectors at each tally point in MCNP:

$$\sigma_{tr,g} = \frac{1}{NV} \sum_n \sum_i \left\{ \left[\sigma(E_i) - (uu' + vv' + ww')_i \sigma(E_i) \right] w_i T_i \right\}, \quad \text{for } E_{g+1} < E_i < E_g \quad (17)$$

where $\hat{\Omega} = \begin{bmatrix} u & v & w \end{bmatrix}^{\mathrm{T}}$ is the direction vector.

This transport cross section was developed and initially tested within the framework of spent fuel storage lattices, but has showed promise for reactor applications (Pounders et al 2005). It is believed, however, that the robustness and accuracy of the Monte Carlo method can be further exploited to yield a transport cross section capable of producing highly accurate diffusion solutions.

CHAPTER 3

DIFFUSION COEFFICIENTS

Several definitions of the diffusion coefficient will now be discussed, as well as their implementation in the Monte Carlo code MCNP5. MCNP5 was chosen since it is the latest release of one of the most popular Monte Carlo codes within the nuclear engineering community, but the following methods are applicable to any Monte Carlo implementation.

3.1. Classical Diffusion Theory

Classical diffusion theory is based on the P_1 approximation to the transport equation. The time-independent multigroup formulation of these equations can be written (Bell and Glasstone, 1979)

$$\nabla \cdot \mathbf{J}_g(\mathbf{r}) + \sigma_g(\mathbf{r})\varphi_g(\mathbf{r}) = \sum_{g'=1}^{G}\left[\sigma_{s,0}^{g'g}(\mathbf{r})\varphi_g(\mathbf{r}) + \chi_g \nu\sigma_{f,g'}(\mathbf{r})\varphi_{g'}(\mathbf{r})\right] \tag{18}$$

$$\nabla\varphi_g(\mathbf{r}) + 3\sigma_g(\mathbf{r})\mathbf{J}_g(\mathbf{r}) = 3\sum_{g'=1}^{G}\sigma_{s,1}^{g'g}(\mathbf{r})\mathbf{J}_{g'}(\mathbf{r}). \tag{19}$$

where $\mathbf{J}(\mathbf{r}) = \int_{4\pi}\hat{\Omega}\psi(\mathbf{r},\hat{\Omega})d\hat{\Omega}$ is the neutron current. The only approximation made in these equations is that the angular flux is linearly anisotropic.

Traditionally, Equation (19) has been recast in a form similar to Fick's law, but this requires the additional approximation that

$$\sum_{g'=1}^{G}\sigma_{s,1}^{g'g}(\mathbf{r})\mathbf{J}_{g'}(\mathbf{r}) = \sum_{g'=1}^{G}\sigma_{s,1}^{gg'}(\mathbf{r})\mathbf{J}_g(\mathbf{r}) \tag{20}$$

(Stamm'ler and Abbate, 1983). This equation is a form of detailed balance which is a good approximation in the presence of heavy scattering. In a purely scattering medium, in fact, this equation is exact. Using this expression in Equation (19) results in

$$\nabla \varphi_g(\mathbf{r}) = -3\left[\sigma_g(\mathbf{r}) - \sum_{g'=1}^{G} \sigma_{s,1}^{gg'}(\mathbf{r})\right]\mathbf{J}_g(\mathbf{r}) \tag{21}$$

The term in brackets is typically defined as the transport cross section, $\sigma_{tr,g}$. This definition of the transport cross section will hereafter be referred to as the 'classical' definition and denoted by a *C* superscript:

$$\sigma_{tr,g}^{C}(\mathbf{r}) = \sigma_g(\mathbf{r}) - \sum_{g'=1}^{G} \sigma_{s,1}^{gg'}(\mathbf{r}). \tag{22}$$

By letting $\sigma_{s,\ell}^{g} = \sum_{g'=1}^{G} \sigma_{s,\ell}^{gg'}(\mathbf{r})$ and defining the average scattering angle as $\bar{\mu}_{0,g} = \frac{\int_{-1}^{1} \mu_0 \sigma_s^g(\mu_0) d\mu_0}{\int_{-1}^{1} \sigma_s^g(\mu_0) d\mu_0}$, Equation (22) can be cast into a more common form:

$$\sigma_{tr,g}^{C}(\mathbf{r}) = \sigma_g(\mathbf{r}) - \bar{\mu}_{0,g}\sigma_{s,0}^{g} \tag{23}$$

Equation (21) is in the form of Fick's law, $\mathbf{J} = -D\nabla\varphi$, implying the following definition of the diffusion coefficient:

$$D_g^C = \frac{1}{3\sigma_{tr,g}^{C}} \tag{24}.$$

The advantage of having the first moment of the P_1 equations in the form of Fick's law is, of course, that it can be substituted into the zeroth moment equation to eliminate the neutron current, resulting in an equation in terms of the scalar flux only. The transport cross section and diffusion coefficient will therefore be treated as equivalent parameters related by $D_g = \left(3\sigma_{tr,g}\right)^{-1}$.

It is the classical definition of the transport cross section that Ilas, G. and Rahnema estimated for spent fuel lattices. Given the tallying capabilities described Section 2.2, however, it can be seen that a Monte Carlo estimate of the classical diffusion coefficient can also be obtained by simply tallying the first Legendre moment of the scattering kernel and subtracting this from the total cross section.

3.2. Flux-Limited Diffusion Theory

Levermore and Pomraning (1981) proposed a "flux-limited" diffusion theory in which the particle current can not exceed the scalar flux (this is not the case in classical diffusion theory.) Flux-limited diffusion theory has been successfully applied to problems in the fields of radiative transfer and radiation hydrodynamics (Olson et al, 2000; Turner and Stone, 2001), but its relevance to reactor physics problems has yet to be investigated.

Through his analysis, Pomraning (1984) derived a new formulation of the transport cross section which may improve upon classical diffusion results. The essence of his formulation is the assumption that the angular flux can be decomposed into a scalar component and normalized angular factor, and furthermore, the normalized angular factor is independent of the energy group. Quantitatively,

$$\psi_g(\mathbf{r},\hat{\Omega}) = \varphi_g(\mathbf{r})\Psi(\mathbf{r},\hat{\Omega}) \tag{25}$$

where $\int_{4\pi} d\hat{\Omega}\Psi(\mathbf{r},\hat{\Omega}) = 1$. This assumption implies that

$$\mathbf{J}_{g'}(\mathbf{r}) = \left(\frac{\varphi_{g'}(\mathbf{r})}{\varphi_g(\mathbf{r})}\right)\mathbf{J}_g(\mathbf{r}) \tag{26}$$

Upon plugging this separation into the second P_1 equation [Equation (19)], the following definition of the transport cross section arises, which will hereafter be denoted by the superscript *FL*:

$$\sigma_{tr,g}^{FL}(\mathbf{r}) = \sigma_g(\mathbf{r}) - \sum_{g'=1}^{G} \frac{\sigma_{s,1}^{g'g}(\mathbf{r})\varphi_{g'}(\mathbf{r})}{\varphi_g(\mathbf{r})}. \tag{27}$$

3.3. An Exact P_1 Diffusion Coefficient

Although the P_1 approximation to the transport equation can often lead to very good results for nuclear reactor cores, the detailed balance approximation of Equation

(20) is dubious, especially in regions of the reactor with strongly absorbing materials. Writing Equation (19) in the form of Fick's law without this approximation yields

$$\nabla \varphi_g(\mathbf{r}) = -3\left[\sigma_g(\mathbf{r}) - \frac{\sum_{g'=1}^{G} \sigma_{s,1}^{g'g}(\mathbf{r})\mathbf{J}_{g'}(\mathbf{r})}{\mathbf{J}_g(\mathbf{r})}\right]\mathbf{J}_g(\mathbf{r}). \qquad (28)$$

Unless this equation is written for only one spatial dimension, the second term in brackets is undefined because of the vector division. Stamm'ler (1983) points out that this term should be seen as a tensor which is necessary in order for the spatial components of the current to vary independently in energy. He further states that this additional complexity is unnecessary in light of the already simplified framework of P_1 theory, and indicates that it is reasonable to replace the current by its magnitude, $J_g(\mathbf{r}) = \left|\mathbf{J}_g(\mathbf{r})\right|$.

With this approximation (or the equivalent assumption of a 1D problem), a transport cross section can be defined that avoids the detailed balance approximation of Equation (20). Since, in one dimension, this cross section leads to the exact solution of the P_1 equations, it will subsequently be denoted by a *P1* superscript:

$$\sigma_{tr,g}^{P1}(\mathbf{r}) = \sigma_g(\mathbf{r}) - \frac{\sum_{g'=1}^{G} \sigma_{s,1}^{g'g}(\mathbf{r})J_{g'}(\mathbf{r})}{J_g(\mathbf{r})}. \qquad (29)$$

In order to implement this definition, it is necessary to calculate the multigroup neutron current, $\mathbf{J}_g(\mathbf{r})$. Within the current context of cross section generation by Monte Carlo methods, this implies calculating a volume-average of the neutron current over the tally cell. This capability is not available in MCNP, but such a tally can be created by recalling the definition of the neutron current:

$$
\begin{aligned}
\overline{\mathbf{J}}_g &= \int_{V_T} dV \mathbf{J}_g(\mathbf{r}) \\
&= \int_{V_T} dV \int_{4\pi} d\hat{\Omega}\hat{\Omega}\psi_g(\mathbf{r},\hat{\Omega}) \\
&= \int_{V_T} dV \int_{4\pi} d\hat{\Omega}\left[\Omega_x\hat{\mathbf{i}} + \Omega_y\hat{\mathbf{j}} + \Omega_z\hat{\mathbf{k}}\right]\psi_g(\mathbf{r},\hat{\Omega}) \\
&= \int_{V_T} dV \int_{4\pi} d\hat{\Omega}\left[\Omega_x\psi_g(\mathbf{r},\hat{\Omega})\hat{\mathbf{i}} + \Omega_y\psi_g(\mathbf{r},\hat{\Omega})\hat{\mathbf{j}} + \Omega_z\psi_g(\mathbf{r},\hat{\Omega})\hat{\mathbf{k}}\right]
\end{aligned}
\tag{30}
$$

where Ω_x, Ω_y and Ω_z are the directional cosines in the *x, y* and *z* directions, respectively, (i.e. $\Omega_x = \hat{\Omega}\cdot\hat{\mathbf{i}}$, etc.). MCNP calculates and stores the directional cosines for each track, therefore a tally can be created for each spatial direction which has the form:

$$
J_{\xi,g} = \frac{1}{NV}\sum_n\sum_i\left[\Omega_{\xi,i}w_iT_i\right], \quad \text{for } E_{g+1} < E_i < E_g \tag{31}
$$

for $\xi \in \{x, y, z\}$.

Now that a current tally has been developed, it is also possible to calculate the current-weighted condensation of the first moment of the scattering kernel consistent with the multigroup derivation [c.f. Equation (6)]. This is an improvement over the flux-weighting approximation of Equation (8). With the current-weighted scattering moment and the avoidance of the detail balance approximation, this definition of the transport cross section has bypassed all the approximations normally associated with classical diffusion theory and should produce the same level of accuracy as direct solution of the P_1 transport equations.

3.4. A High Order Diffusion Coefficient

All previous definitions of the diffusion coefficient have truncated the P_N equations at $N = 1$, neglecting higher order terms, and used the first moment equation to express the neutron current in terms of the flux gradient (an expression of Fick's Law). These expressions are of course only approximate closures to the transport equation since they neglect information carried by the higher order moments. It seems unduly wasteful, however, to be limited to the assumption of linear anisotropy when working within the

context of Monte Carlo methods. The high-order accuracy of the Monte Carlo method should be exploited as much as possible when computing a diffusion coefficient.

Consider instead an exact solution of Fick's Law as a closure to the transport equation. That is, instead of postulating an expression of Fick's Law based on the P_1 equation, assume that Fick's Law is an *a priori* valid relationship and solve for the diffusion coefficient in terms of a stochastically computed current and flux gradient.

Integrating Fick's Law over a tally cell and dividing by the volume, V_T, one has

$$\frac{1}{V_T}\int_{V_T} dV\, \mathbf{J}_g(\mathbf{r}) = -\frac{1}{V_T}\int_{V_T} dV\, D_g(\mathbf{r})\nabla\varphi_g(\mathbf{r})\,. \tag{32}$$

If it is assumed that V_T is a small and homogenous cell in which the diffusion coefficient is constant, Equation (32) can be written

$$\frac{1}{V_T}\int_{V_T} dV\, \mathbf{J}_g(\mathbf{r}) = -\frac{D_g}{V_T}\int_{V_T} dV\, \nabla\varphi_g(\mathbf{r})\,. \tag{33}$$

The left-hand side of this expression is the average current within the cell, which can be tallied by Equation (31). The right-hand side can be simplified using a special case of the divergence theorem to yield

$$\overline{\mathbf{J}}_g V_T = -D_g\int_{\partial V_T} \hat{\mathbf{n}} ds\, \varphi_g(\mathbf{r}) \tag{34}$$

where ∂V_T is the bounding surface of V_T containing the unit area s with outward normal $\hat{\mathbf{n}}$. The right-hand side is the surface-integrated flux for all bounding surfaces, a value which can be tallied using a surface-flux tally that is a standard feature in MCNP.

Since Equation (34) is a vector equation, special care must be given to the calculation of D_g. If the diffusion coefficient is forced to be a scalar constant then Equation (34) will be exact only if the ratio of the current to the flux gradient is the same for each spatial direction—an assumption will almost certainly be untrue in three dimensions. One option which will preserve the ratio in all dimensions is to take D_g to be the diagonal matrix

$$D_g = \begin{bmatrix} D_{x,g} & 0 & 0 \\ 0 & D_{y,g} & 0 \\ 0 & 0 & D_{z,g} \end{bmatrix} \tag{35}$$

where the diagonal elements are directional diffusion coefficients for the three spatial dimensions x, y and z. One particularly nice aspect of this formulation is that it allows one to calculate an independent axial diffusion coefficient for 3D systems. This would be particularly useful for cases where streaming along a particular direction is of concern (i.e. dominant) such as the CANDU reactor with voided channels, for which the axial streaming is known to be poorly treated by classical diffusion theory.

Many diffusion codes, however, do not make allowances for directional diffusion coefficients, so some sort of averaging must be performed to combine two or three of the directions. In one dimension, however, the solution of Equation (34) is trivial. As a preliminary investigation, therefore, the focus will be on the one dimensional case, which can be written

$$D_g^S = -\frac{\overline{\mathbf{J}}_g V_T}{\left(\overline{\varphi}_g^+ - \overline{\varphi}_g^-\right) \cdot A_T} \tag{36}$$

where $\overline{\varphi}^+$ and $\overline{\varphi}^-$ are the surface-averaged fluxes averaged over the right and left boundaries of the tally cell, respectively, and the superscript S on the diffusion coefficient denotes the fact this definition relies only on the stochastic solutions of the current and flux.

There is one final caveat about this formulation. The tally cell volume, V_T, must be small in the sense that the flux gradient should be approximately linear across it. If this is not the case then the denominator of Equation (36) will be a poor estimate of the actual flux gradient.

An alternative way of looking at this requirement is to notice that when proceeding from Equation (32) to Equation (33) the assumption was made that the diffusion coefficient was constant within the tally cell. In actuality there will be

variations in the diffusion coefficient due to gradient variations within the cell. Comparing Equations (32) and (33) it can be seen that the constant diffusion coefficient (denoted here as $\bar{D}_g$) is implicitly defined as

$$\bar{D}_g = \frac{\int_{V_T} dV\, D_g(\mathbf{r}) \nabla \varphi_g(\mathbf{r})}{\int_{V_T} dV\, \nabla \varphi_g(\mathbf{r})}. \tag{37}$$

If the spatial flux distribution is approximately linear (i.e. constant gradient) then the flux terms in the numerator and denominator cancel and the definition results in a simple average. Otherwise the diffusion coefficient will be weighted with the flux gradient over the cell volume, which will lead to inconsistent results.

CHAPTER 4

RESULTS

Several configurations of a one dimensional reactor core were solved using the diffusion coefficients described in the previous section. These problems exhibit a varying degree of heterogeneity that will aid in determining the accuracy and applicability of each diffusion method. Before proceeding to the results, however, a validation of the stochastic cross section generation routines will be shown.

4.1. Cross Section Validation

The methods described in Section 2.2 for generating stochastic cross sections were implemented in MCNP5. In order to verify that the implementation was functioning properly, 3-group cross sections were generated from a fine-group library for a 2D BWR pin cell. The condensed cross section set tallied by the modified version of MCNP was checked against an analytic calculation of the cross sections using the fine-group cross sections and MCNP output fluxes. Next, as a point of reference and comparison, the collision probability code HELIOS (Casal et al, 2003) was used to generate the same cross section set as an external validation. Both MCNP and HELIOS used the standard 47-group HELIOS library for the condensation to ensure a consistent comparison.

The benchmark is a multigroup version of the problem previously published by Rahnema et al (1997). The problem is a 1.6 cm square BWR pin cell consisting of fuel, clad and moderator. The fuel region is subdivided into 5 annular cross section regions to avoid spectral homogenization (see Section 2.2). The problem geometry is shown in Appendix A.

Tables 1 and 2 compare the MCNP-collapsed cross section against those computed analytically outside of MCNP. The RMS average of the errors in the five fuel regions have been shown for brevity. It can be seen that there are no statistically significant (within 3σ) errors. This indicates that MCNP has been successfully modified to accurately tally condensed multigroup cross sections.

Table 1: Analytic vs. Stochastic Cross Sections

	Group	Σ_{tr}	Σ_{ab}	Σ_{fi}	$\nu\Sigma_{fi}$
RMS Fuel PD**	1	0.01% (0.02%)	0.02% (0.03%)	0.04% (0.04%)	0.05% (0.04%)
	2	0.00% (0.03%)	0.02% (0.02%)	0.01% (0.02%)	0.01% (0.02%)
	3	0.00% (0.02%)	0.01% (0.02%)	0.01% (0.02%)	0.01% (0.03%)
Clad PD	1	0.01% (0.02%)	0.01% (0.02%)	Non-fissionable materials	
	2	0.00% (0.02%)	0.01% (0.02%)		
	3	0.00% (0.02%)	0.00% (0.02%)		
Water PD	1	0.01% (0.06%)	-0.06% (0.44%)		
	2	0.00% (0.03%)	0.02% (0.05%)		
	3	0.00% (0.04%)	0.00% (0.04%)		

*The parenthetical values are the statistical uncertainties corresponding to one standard deviation
**Percent difference = $|\Sigma_{MCNP} - \Sigma_{EXACT}| / \Sigma_{EXACT}$

Table 2: Analytic vs. Stochastic P0 Scattering Matrices

		Outgoing groups		
	RMS Fuel	1	2	3
Incoming groups	1	0.01% (0.02%)	0.11% (1.34%)	0.00% (0.00%)
	2	0.00% (0.00%)	0.00% (0.02%)	0.11% (0.09%)
	3	0.00% (0.00%)	0.19% (0.13%)	0.00% (0.02%)
	Clad	1	2	3
	1	0.01% (0.02%)	0.14% (2.30%)	0.00% (0.00%)
	2	0.00% (0.00%)	0.00% (0.02%)	0.10% (0.12%)
	3	0.00% (0.00%)	-0.03% (0.14%)	0.00% (0.02%)
	Water	1	2	3
	1	0.01% (0.08%)	0.02% (0.11%)	0.00% (0.00%)
	2	0.00% (0.00%)	0.00% (0.03%)	0.03% (0.07%)
	3	0.00% (0.00%)	-0.05% (0.59%)	0.00% (0.04%)

*The parenthetical values are the statistical uncertainties corresponding to one standard deviation
**Error = $|\Sigma_{MCNP} - \Sigma_{EXACT}| / \Sigma_{EXACT}$

Tables 3 and 4 compare the cross sections generated by MCNP with the cross sections generated HELIOS. Overall there is very good cross section agreement, but there are significant differences in the fast group fuel cross sections. Upon closer examination these cross section differences can be attributed to differences in the calculated flux spectra for these regions, which are plotted in Figure 1. These flux differences arise from the difficulty of accurately treating specularly reflective boundary conditions with the collision probability method for such a small system. Since the Monte Carlo method does not have this limitation (associated with numerical integrations), it is capable of producing a more accurate flux spectrum for collapsing the cross sections.

Table 3: MCNP vs. HELIOS Cross Section Differences

	Group	Σ_{tr}	Σ_{ab}	Σ_{fi}	$\nu\Sigma_{fi}$
RMS Fuel PD**	1	0.23% (0.05%)*	0.34% (0.02%)	0.59% (0.02%)	0.63% (0.02%)
	2	0.00% (0.02%)	0.01% (0.02%)	0.01% (0.01%)	0.01% (0.01%)
	3	0.02% (0.01%)	0.03% (0.01%)	0.03% (0.01%)	0.03% (0.01%)
Clad PD	1	0.04% (0.02%)	0.04% (0.02%)	Non-fissionable materials	
	2	0.00% (0.01%)	0.02% (0.01%)		
	3	0.00% (0.01%)	0.03% (0.01%)		
Water PD	1	0.06% (0.06%)	0.49% (0.44%)		
	2	0.00% (0.03%)	0.00% (0.04%)		
	3	0.05% (0.03%)	0.06% (0.04%)		

*The parenthetical values are the statistical uncertainties corresponding to one standard deviation

**Percent difference = $|\Sigma_{HELIOS} - \Sigma_{MCNP}| / \Sigma_{MCNP}$

Table 4: MCNP vs. HELIOS P0 Scattering Matrix Differences

		Outgoing groups					
	RMS Fuel	1		2		3	
Incoming groups	1	0.24%	(0.01%)*	0.60%	(0.11%)	0.00%	(0.00%)
	2	0.00%	(0.00%)	0.00%	(0.01%)	0.06%	(0.05%)
	3	0.00%	(0.00%)	0.22%	(0.09%)	0.00%	(0.01%)
	Clad	1		2		3	
	1	0.04%	(0.02%)	0.27%	(0.22%)	0.00%	(0.00%)
	2	0.00%	(0.00%)	0.00%	(0.01%)	0.05%	(0.10%)
	3	0.00%	(0.00%)	0.06%	(0.12%)	0.00%	(0.01%)
	Water	1		2		3	
	1	0.04%	(0.08%)	0.11%	(0.11%)	0.00%	(0.00%)
	2	0.00%	(0.00%)	0.00%	(0.03%)	0.00%	(0.07%)
	3	0.00%	(0.00%)	0.23%	(0.58%)	0.05%	(0.04%)

*The parenthetical values are the statistical uncertainties corresponding to one standard deviation

**Error = $|\Sigma_{HELIOS} - \Sigma_{MCNP}| / \Sigma_{MCNP}$

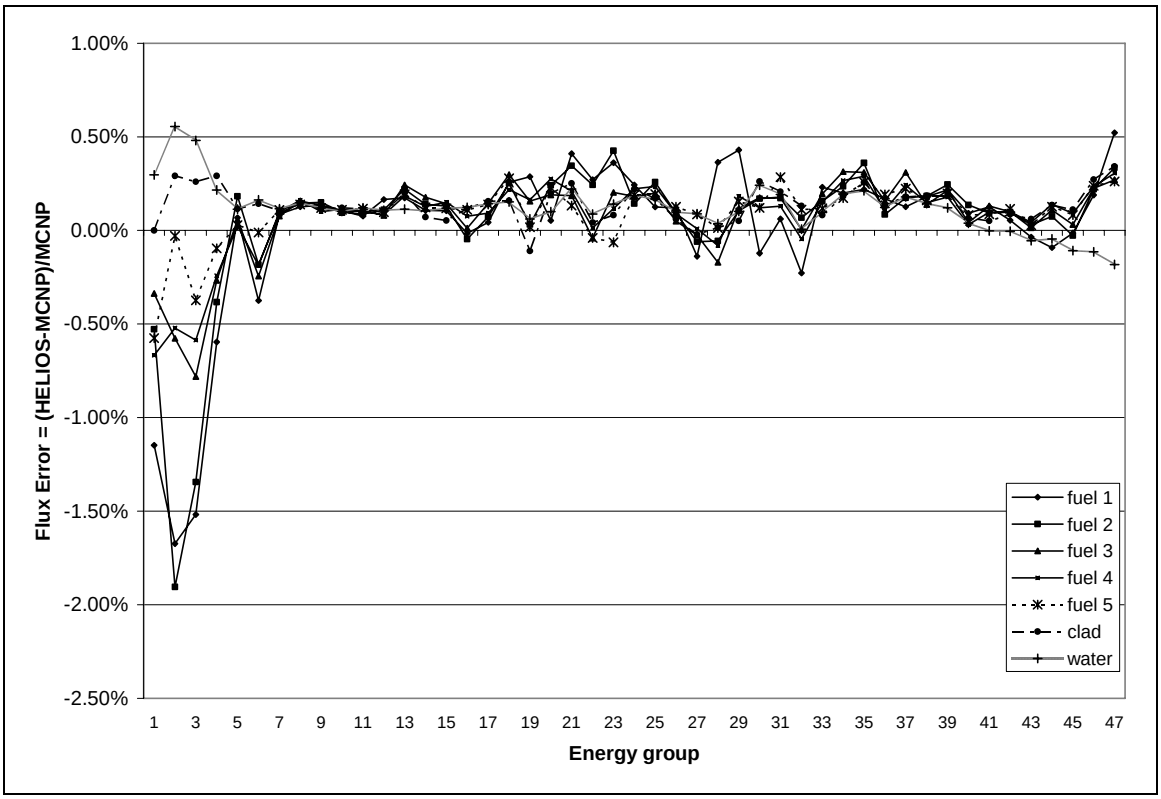

Figure 1: HELIOS vs. MCNP Relative Fine-Group Flux Errors

4.2. Fine-Mesh Diffusion

Attention will now be turned to examining the various diffusion coefficients defined in Chapter 3. A simplified 1D BWR reactor core was chosen as a benchmark problem so that the underlying properties of the diffusion methods can be examined without unnecessary complexity. The benchmark problem was taken from Ilas, D. and Rahnema (2003) and fundamentally consists of four unique assembly types. Each assembly consists of 4 homogeneous fuel regions sandwiched between two homogenous coolant/clad channels. These assemblies are arranged in three different 7-assembly configurations to form cores of varying heterogeneity. The assembly and core geometries are shown in Appendix B.

Core configuration 1 is the simplest core, with only slightly varying enrichment and no burnable absorber elements. Core configurations 2 and 3 are more difficult cases, containing increasing amounts of gadolinium in alternating assemblies. This test suite allows the diffusion coefficients to be tested in a range of problems with varying difficulty.

Diffusion Without Group Condensation

In order to capture only the errors associated with using diffusion theory instead of transport theory, a number of problems were solved in order of increasing complexity. First, the four assemblies with specularly reflective boundary conditions were solved in two groups. The transport and diffusion solutions were both in two groups to ensure that there were no errors arising from group condensation.

After HELIOS was used to generate a 2-group material library, MCNP generated solutions for all four fuel assemblies and tallied diffusion coefficients for each material region. The diffusion code NESTLE (Turinksy et al, 1994) was then used to solve the

four assemblies with the same 2-group library while varying the diffusion coefficients over the range of definitions previously discussed.

Table 5 displays the reference eigenvalues and the eigenvalue errors associated with the different diffusion theories for all four assemblies. Since there was no cross section collapsing, these errors are a result only of using the diffusion approximation instead of full transport theory. In all cases the stochastic diffusion coefficient, D^S, outperforms the others by a significant margin. The flux-limited coefficient seems to fare the worst.

Table 5: Assembly Eigenvalue Differences (2G Diffusion v. 2G Transport)

		Δk_{eff}^* [mk]			
Assembly	$k_{eff} \pm 0.03$ mk	D^C	D^{FL}	D^{P1}	D^S
1	1.18099	1.24	1.97	1.39	0.29
2	1.23736	1.17	2.07	1.40	0.03
3	0.61445	-6.14	-9.89	-6.26	-4.77
4	0.31073	-0.56	-0.52	-0.40	-0.07

*$\Delta k_{eff} = [k_{\text{DIFFUSION}} - k_{\text{MCNP}}]$*1000 mk

Table 6 displays the average, root-mean-square, mean relative and maximum errors for the region-wise fission densities for the four assemblies (see Appendix C for specific definitions of these statistics.) The classical, flux-limited and P_1 coefficients all perform comparably. The stochastic diffusion coefficient exhibits the lowest fission errors in all cases.

Table 6: Assembly Fission Density Error Statistics (2G Diffusion v. 2G Transport)

Assembly	Method	AVG	RMS	MRE	MAX
1	D^C	0.10%	0.10%	0.10%	0.12%
	D^{FL}	0.19%	0.20%	0.19%	0.24%
	D^{P1}	0.30%	0.33%	0.29%	0.44%
	D^S	0.10%	0.10%	0.10%	0.12%
2	D^C	0.26%	0.31%	0.20%	0.42%
	D^{FL}	0.09%	0.11%	0.07%	0.16%
	D^{P1}	0.31%	0.35%	0.24%	0.47%
	D^S	0.06%	0.06%	0.06%	0.06%
3	D^C	1.52%	1.53%	1.60%	1.69%
	D^{FL}	2.12%	2.14%	2.26%	2.42%
	D^{P1}	1.54%	1.55%	1.62%	1.72%
	D^S	1.01%	1.05%	1.15%	1.30%
4	D^C	0.29%	0.34%	0.28%	0.47%
	D^{FL}	0.15%	0.17%	0.14%	0.24%
	D^{P1}	0.28%	0.32%	0.27%	0.44%
	D^S	0.12%	0.15%	0.12%	0.21%

*Average 1σ uncertainty associated with reference fission densities ~0.02%

Next, the three core configurations were examined. Again, a two-group library was generated by HELIOS, then MCNP was used to generate a transport solution and compute diffusion coefficients. NESTLE then solved the cores using the various diffusion coefficients.

All diffusion methods do relatively well on configuration 1, since it contains no strong absorbers and has slowly varying material properties. The average error increases as expected for configurations 2 and 3, but the high order method using D^S does well for all three configurations—an order of magnitude better for configuration 3, in fact.

Table 7: Core Eigenvalue Differences (2G Diffusion v. 2G Transport)

Configuration	$k_{eff} \pm 0.03$ mk	Δk_{eff}^{*} [mk]			
		D^C	D^{FL}	D^{P1}	D^S
1	1.16818	0.92	1.22	1.57	1.00
2	0.94224	-3.47	-3.55	-3.83	-1.11
3	0.78916	-6.53	-7.04	-6.07	-0.64

*$\Delta k_{eff} = [k_{\text{DIFFUSION}} - k_{\text{MCNP}}]$*1000 mk

Table 8 displays the fission density error statistics of the three cores. In spite of the high order method producing more accurate eigenvalues, it is not discernibly better than any other method with respect to fission densities. In fact, the maximum error for configuration 3 is markedly higher at 9.3%.

Table 8: Core Fission Density Error Statistics (2G Diffusion v. 2G Transport)

Configuration	Method	AVG	RMS	MRE	MAX
1	D^C	0.55%	0.82%	0.35%	2.33%
	D^{FL}	0.53%	0.88%	0.28%	2.71%
	D^{P1}	0.64%	0.97%	0.40%	2.90%
	D^S	0.64%	1.04%	0.38%	3.42%
2	D^C	1.32%	1.61%	0.74%	3.25%
	D^{FL}	1.64%	2.05%	0.85%	4.10%
	D^{P1}	1.39%	1.77%	0.77%	3.94%
	D^S	0.92%	1.40%	0.59%	4.14%
3	D^C	2.08%	2.31%	1.41%	4.24%
	D^{FL}	2.15%	2.71%	1.23%	5.37%
	D^{P1}	2.09%	2.49%	1.42%	5.06%
	D^S	2.40%	3.72%	1.43%	9.25%

*Average 1σ uncertainity associated with reference fission densities ~0.02%

The fission density error distributions for configurations 1 and 3 are shown in Figures 2 and 3. The classical, flux-limited and P_1 diffusion theories all exhibit a similar

error trend. The stochastic diffusion method has a distinctly different distribution that is more accurate for the central assemblies, but deviates significantly towards the boundary. In spite of having large maximum fission density errors, the stochastic diffusion method has an order of magnitude better estimate of the eigenvalue. It accurately predicts the fission densities for the central high-power assemblies, even though it deviates towards the extremities.

These different tendencies signify that the stochastically defined diffusion coefficient is fundamentally different than the other three. The classical, flux-limited and P_1 diffusion coefficients are all strong functions of the cross sections, namely the total and the first scattering moment cross sections. With no collapsing the classical diffusion coefficient is a function of *only* these cross sections with no flux dependency, while the flux-limited and P_1 coefficients can be seen as being similar to the classical coefficient, but with various spectrum-dependent adjustments. These coefficients are therefore strongly tied to the material.

The stochastic diffusion coefficient, on the other hand, is not explicitly dependent on the system cross sections; the dependence is implicit through the current and flux gradient within a cell. This coefficient is a strong function of the local flux distribution. The benefit of this strong dependency is that it carries more information about the neutron flow to the diffusion calculation. Caution must be taken in regions with sharp flux gradients, however, since the tallies of the current and flux gradient represent averages and are only first order accurate by definition (see Section 3.4).

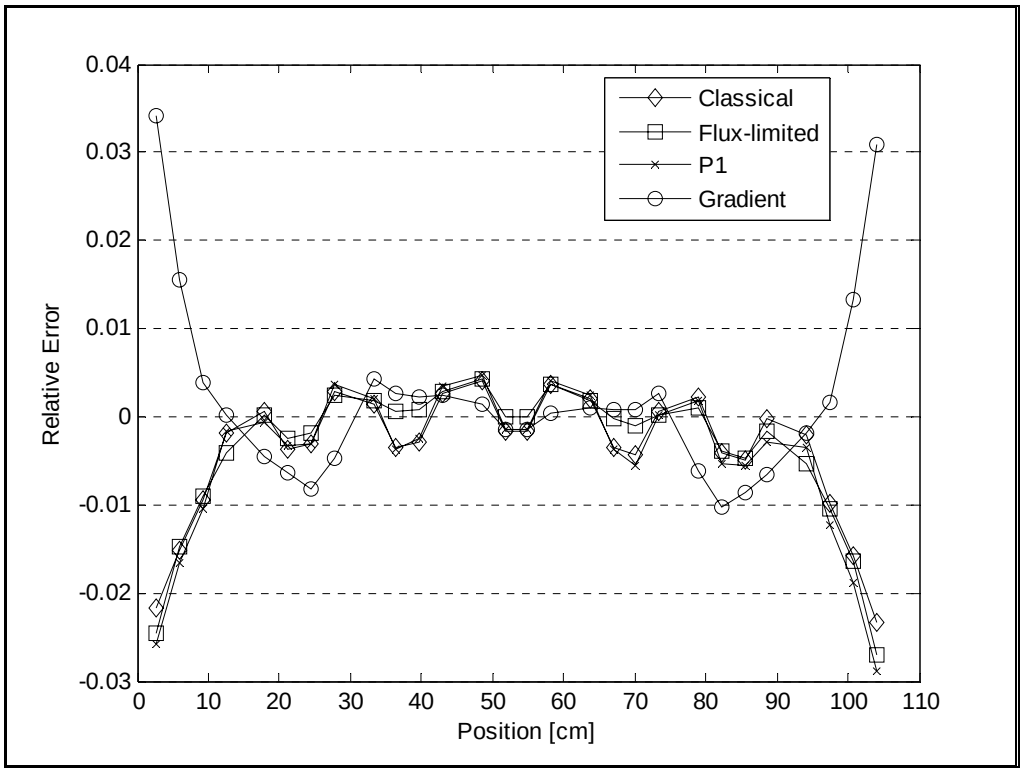

Figure 2: Fission Density Error Distributions for Configuration 1

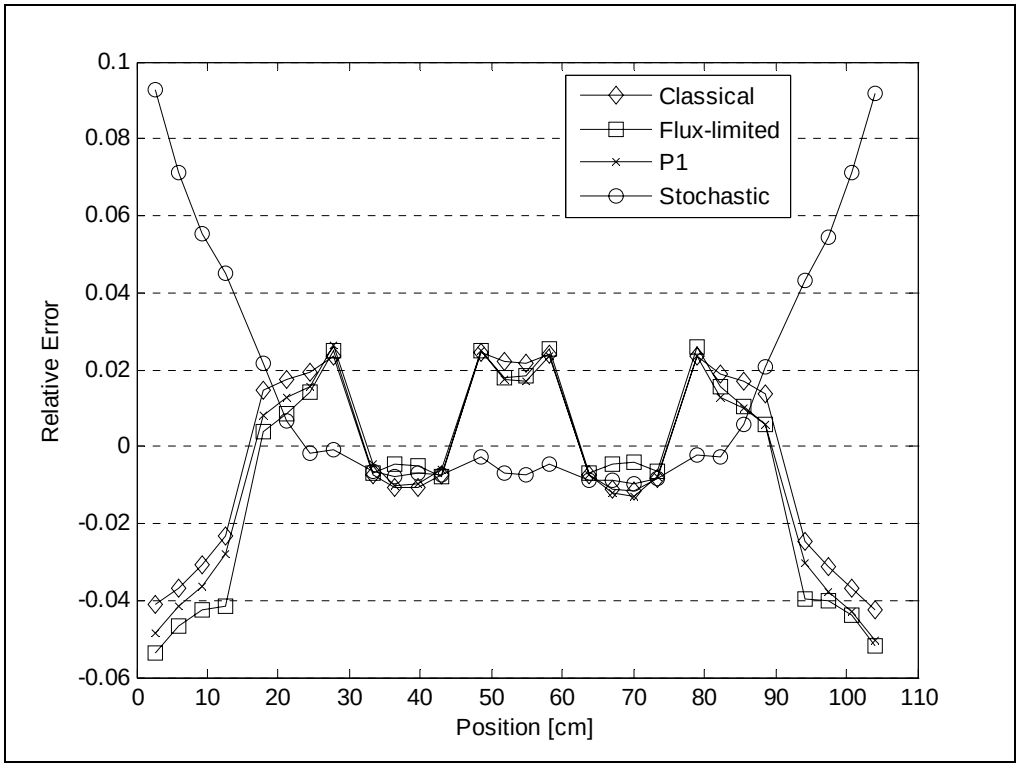

Figure 3: Fission Density Error Distributions for Configuration 3

Since the fission density errors are strongly influenced by errors in the thermal flux, they are not a good indicator of how the different diffusion coefficients perform at higher energies. The group flux errors for configuration 3 will therefore be examined in more depth. Configuration 3 will be examined since the regions with heavy gadolinium additions exhibit harder spectra and should highlight errors associated with the fast flux.

Figure 4 shows the fast flux error distribution. The stochastic diffusion coefficient produces a solution that deviates sharply towards the boundary, but is otherwise very accurate. The classical diffusion coefficient produces the best answer in the fast group in the assembly adjacent to the boundary. Beyond the first assembly, however, the flux-limited and P_1 coefficients perform better.

Similar trends are observed near the boundary in the thermal group in Figure 5. Away from the boundary, the coefficients perform more or less comparably, but the flux-limited errors peak substantially in the water regions at assembly boundaries.

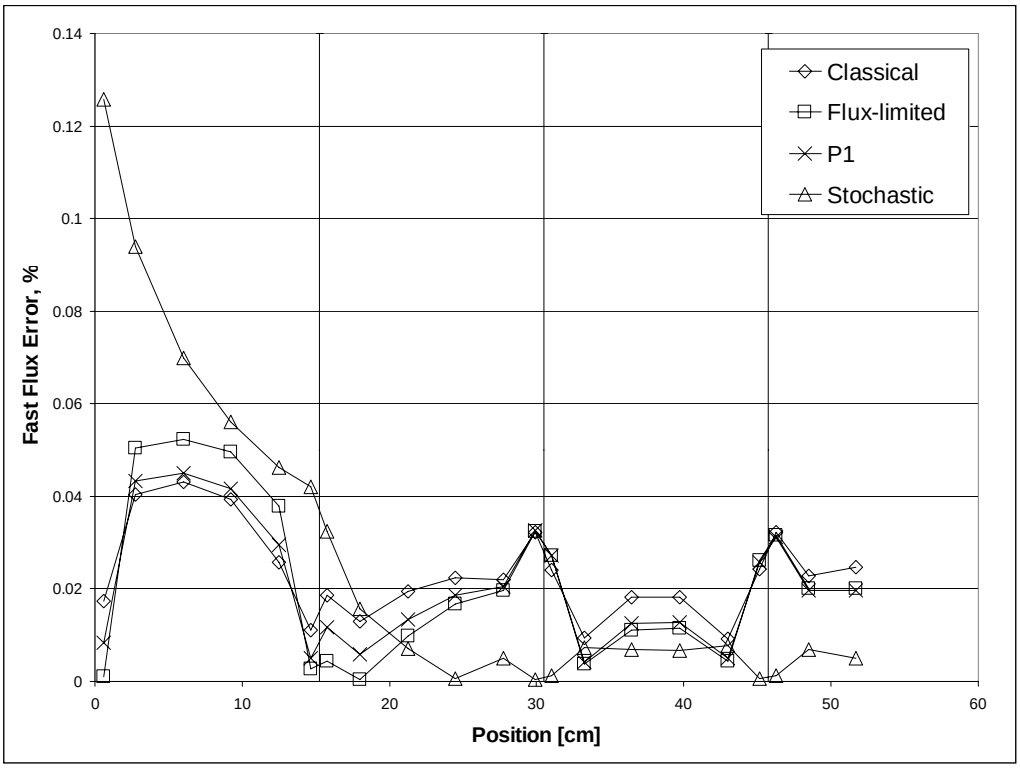

Figure 4: Fast Flux Error Distribution for Core 3

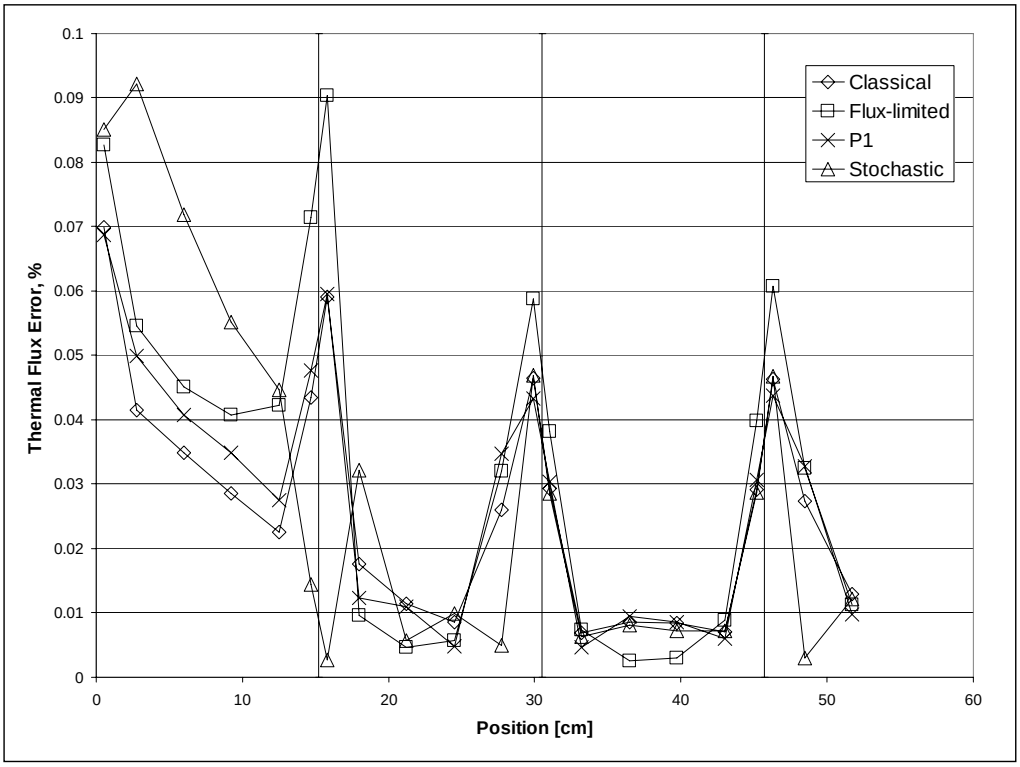

Figure 5: Thermal Flux Error Distribution for Core 3

To investigate how sensitive these results are to the mesh size (i.e. the region volumes which are considered to have linear flux gradients and flat currents), the calculation for configuration 3 was repeated with each material region divided in two tally regions. The results follow in Tables 9 and 10. It can be seen that the eigenvalue error for the stochastic coefficient is approximately halved and there was a moderate decrease in error for the fission densities. This indicates that decreasing the cross section mesh does improve the solution, but the stochastic method still struggles more than the others near boundaries due to its strong dependence on spatial variations in the flux. The other coefficients did not change appreciably, which was expected because of their strong material dependence.

Table 9: Eigenvalue Differences for Halved Mesh (2G Diffusion v. 2G Transport)

	Δk_{eff}^{*} [mk]			
$k_{eff} \pm 0.03$ mk	D^C	D^{FL}	D^{P1}	D^S
1.16726	0.89	1.58	1.1	1.1
0.94224	-3.57	-3.63	-3.66	0.16
0.78916	-6.58	-5.83	-6.96	0.36

*$\Delta k_{eff} = [k_{\text{DIFFUSION}} - k_{\text{MCNP}}]$*1000 mk

Table 10: Fission Density Error Statistics for Halved Mesh (2G Diffusion v. 2G Transport)

Configuration	Method	AVG	RMS	MRE	MAX
1	D^C	0.55%	0.82%	0.36%	2.29%
	D^{FL}	0.53%	0.88%	0.28%	2.63%
	D^{P1}	0.63%	0.94%	0.40%	2.59%
	D^S	0.63%	1.15%	0.31%	3.93%
2	D^C	1.32%	1.61%	0.75%	3.29%
	D^{FL}	1.66%	2.09%	0.86%	4.18%
	D^{P1}	1.44%	1.83%	0.80%	3.99%
	D^S	1.17%	1.80%	0.65%	5.31%
3	D^C	2.09%	2.33%	1.42%	4.39%
	D^{FL}	2.14%	2.72%	1.22%	5.51%
	D^{P1}	2.12%	2.56%	1.44%	5.15%
	D^S	2.16%	3.40%	1.20%	8.87%

*Average 1σ uncertainity associated with reference fission densities ~0.02%

Infinite-Medium Cross Sections

The previous results provide valuable insight into the behavior of the different diffusion coefficients, but have limited usefulness for practical reactor physics problems since it has been assumed that the full-core transport solution is known. It is common practice to sub-divide reactor cores into repeating cells (usually fuel assemblies) and seek a solution for each unique assembly with approximate boundary conditions that simulate the boundary conditions it will see inside the core (specularly reflective, for example).

The current core configurations were analyzed in a similar manner. Each core contains two unique assembly types. These single assemblies were solved with specular reflection in MCNP to generate material-wise diffusion coefficients, then the entire cores were solved using the 'infinite-medium' diffusion coefficients. Tables 11 and 12 summarize the errors associated with these calculations.

As was expected, since the classical diffusion coefficient does not depend on the flux spectrum or spatial distribution, there are no additional errors associated with the infinite medium diffusion coefficients. The flux-limited and P_1 coefficients do not produce significantly different results in this case either, indicating that the energy spectrum is sufficiently conserved when the infinite medium calculations are performed.

The stochastic diffusion coefficient does much more poorly in this case, however. This is to be expected since it so strongly depends on the spatial distribution of the flux. Changing the boundary conditions on these small assemblies significantly alters local flux gradients near the boundaries. This in turn creates diffusion coefficients that do not perform well in the full-core calculations.

Table 11: Eigenvalue Differences with Infinite-Medium Diffusion Coefficients (2G Diffusion v. 2G Transport)

		Δk_{eff}^{*} [mk]			
Configuration	$k_{eff} \pm 0.03$ mk	D^C	D^{FL}	D^{P1}	D^S
1	1.16818	1.04	1.48	1.53	6.8
2	0.94224	-3.87	-3.88	-2.52	27.58
3	0.78916	-6.85	-6.99	-3.66	46.64

*$\Delta k_{eff} = [k_{\text{DIFFUSION}} - k_{\text{MCNP}}]$*1000 mk

Table 12: Fission Density Error Statistics with Infinite-Medium Diffusion Coefficients (2G Diffusion v. 2G Transport)

Configuration	Method	AVG	RMS	MRE	MAX
1	D^C	0.90%	1.26%	0.49%	3.25%
	D^{FL}	1.04%	1.56%	0.53%	4.10%
	D^{P1}	1.04%	1.46%	0.57%	3.94%
	D^S	1.38%	1.88%	1.04%	5.58%
2	D^C	1.43%	1.72%	0.83%	3.36%
	D^{FL}	1.83%	2.18%	1.09%	4.10%
	D^{P1}	1.47%	1.81%	0.83%	3.94%
	D^S	7.94%	10.39%	7.34%	19.67%
3	D^C	2.25%	2.48%	1.58%	4.37%
	D^{FL}	2.41%	2.85%	1.59%	5.17%
	D^{P1}	2.21%	2.88%	1.33%	5.79%
	D^S	15.29%	16.03%	12.30%	21.97%

*Average 1σ uncertainity associated with reference fission densities ~0.02%

Diffusion With Group Condensation

We will now briefly look at the above diffusion methods coupled with group condensation. The same three core configurations analyzed above were solved again, but this time the 47-group library from HELIOS was used. Condensed 2-group cross sections and diffusion coefficients were tallied for each material region in the three cores. The two-group libraries and diffusion coefficients were then used to solve the three configurations with NESTLE, and the results were compared against the 47-group reference solutions.

Table 13 shows the diffusion eigenvalue errors associated with the four diffusion coefficients, followed by Table 14 showing the fission density error statistics. In the context of group condensation, the P_1 and stochastic methods seem to perform much better. The classical and flux-limited coefficients most likely do so poorly because of spectral homogenization errors, where the energy spectrum was collapsed (tallied) over too broad an area (see Section 2.2). The stochastic diffusion coefficient performs better perhaps because it relies more on the spatial distribution of neutrons rather than the energy distribution and avoids errors associated with collapsing cross sections.

Table 13: Eigenvalue Differences (2G Diffusion v. 47G Transport)

		Δk_{eff}^{*} [mk]			
Configuration	$k_{eff} \pm 0.03$ mk	D^C	D^{FL}	D^{P1}	D^S
1	1.15843	10.84	11.37	1.72	2.16
2	0.90963	17.81	17.48	-0.52	4.22
3	0.72587	26.72	27.00	-5.00	6.29

*$\Delta k_{eff} = [k_{\text{DIFFUSION}} - k_{\text{MCNP}}]$*1000 mk

Table 14: Fission Density Error Statistics (2G Diffusion v. 47G Transport)

Configuration	Method	AVG	RMS	MRE	MAX
1	D^C	3.15%	4.17%	2.31%	10.51%
	D^{FL}	3.30%	4.35%	2.44%	10.85%
	D^{P1}	0.99%	1.23%	0.78%	2.76%
	D^S	0.81%	1.22%	0.53%	3.85%
2	D^C	8.02%	9.86%	6.55%	17.97%
	D^{FL}	8.37%	10.39%	6.88%	18.61%
	D^{P1}	2.08%	2.36%	1.86%	4.06%
	D^S	1.49%	2.07%	1.03%	5.06%
3	D^C	12.81%	15.07%	10.77%	25.77%
	D^{FL}	13.36%	15.69%	11.24%	26.74%
	D^{P1}	1.94%	2.59%	1.84%	5.22%
	D^S	2.93%	3.97%	1.82%	8.76%

*Average 1σ uncertainity associated with reference fission densities ~0.02%

CHAPTER 5

CONCLUSIONS

Several definitions of the diffusion coefficient have been analyzed in an attempt to ascertain the most accurate way of computing a diffusion solution for reactor physics problems. The classical, flux-limited and P_1 diffusion coefficients performed comparably for all test problems. This indicates that the primary source of diffusion error is the limitation imposed by the P_1 equations that the flux is linearly anisotropic. The intermediate assumptions associated with the classical or flux-limited derivation of the transport cross section seem to be secondary to this approximation. These approximations, however, tended to improve the performance of diffusion methods at fast energies and in highly absorbing media.

The stochastic diffusion coefficient represents a fundamentally different form of closure of the transport equation. Overall this coefficient performed much better, but its strong dependence on the spatial flux distribution makes it harder to implement in a manner which is practical for reactor physics problems.

There is much work that remains in this area. This thesis has revealed that there exists a diffusion methodology which is capable of superseding P_1 theory, but a practical implementation requires more investigation. Simulating leakage may allow high order diffusion coefficients to be calculated, similar to performing buckling searches in B_N theory, but it is advantageous to make the most of the Monte Carlo Method, avoiding unnecessary approximations or series truncations that frequently accompany deterministic methods.

APPENDIX A

BWR PIN CELL BENCHMARK

The BWR pin cell benchmark was taken from Rahnema, Ilas and Sitaraman (1997). The problem consists of a square cell containing 2.80% enriched $U0_2$ pin with natural zirconium cladding surrounding by moderator. The moderator is H_20 at 300 K. The geometry is shown in Figure 4, with dimensions following in Table 13.

The fuel region was subdivided into five annular regions only for the purpose of generating cross sections. The materials and densities in these regions are constant.

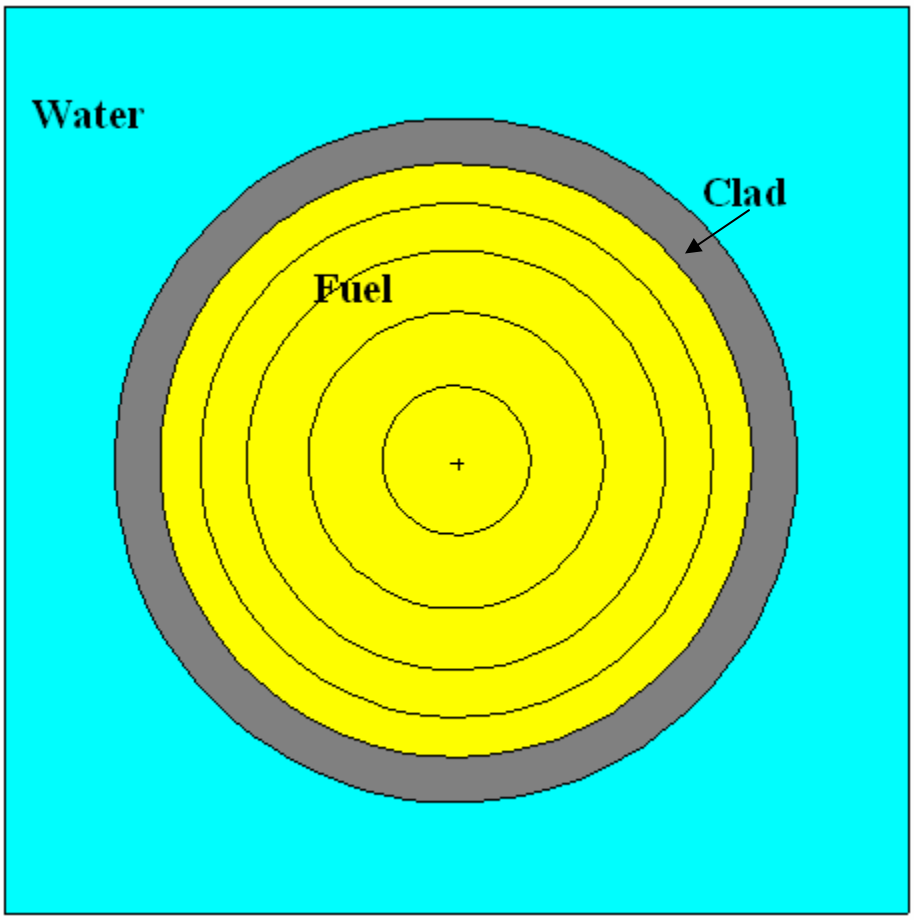

Figure 6: Pin Cell Geometry with Cross Section Meshing

Table 15: Pin Cell Dimensions

Cell Pitch, *P*	1.6256 cm
Fuel Outer Radius, RO	0.61341 cm
Fuel Inner Radius, RI	0.53213 cm

APPENDIX B

ONE DIMENSIONAL SIMPLIFIED BWR CORE

The geometry of the one-dimensional BWR core was taken from Ilas D. and Rahnema (2003). Figure 5 shows the core composition and geometry. Each material region is homogeneous and uniform. Table 10 summarizes the dimensions of the core

The 'water' is actually a coolant and zirconium mixture. Fuel I and fuel II are 2.2% and 3.6% enriched UO_2, respectively, mixed with light water and zirconium. Fuel + Gd is a fuel, zirconium and water mixture with 4.0% enriched uranium and 4% gadolinium. Vacuum boundary conditions were assigned to the left and right boundaries.

Each core can be divided into seven fuel assemblies. An assembly consists of four contiguous fuel regions with a region of water on either side. Each core therefore contains two unique assembly types which appear in an alternating pattern.

Table 16: Core Dimensions

Water slab width	1.1176 cm
Fuel slab width	3.2512 cm
Total core width	106.68 cm

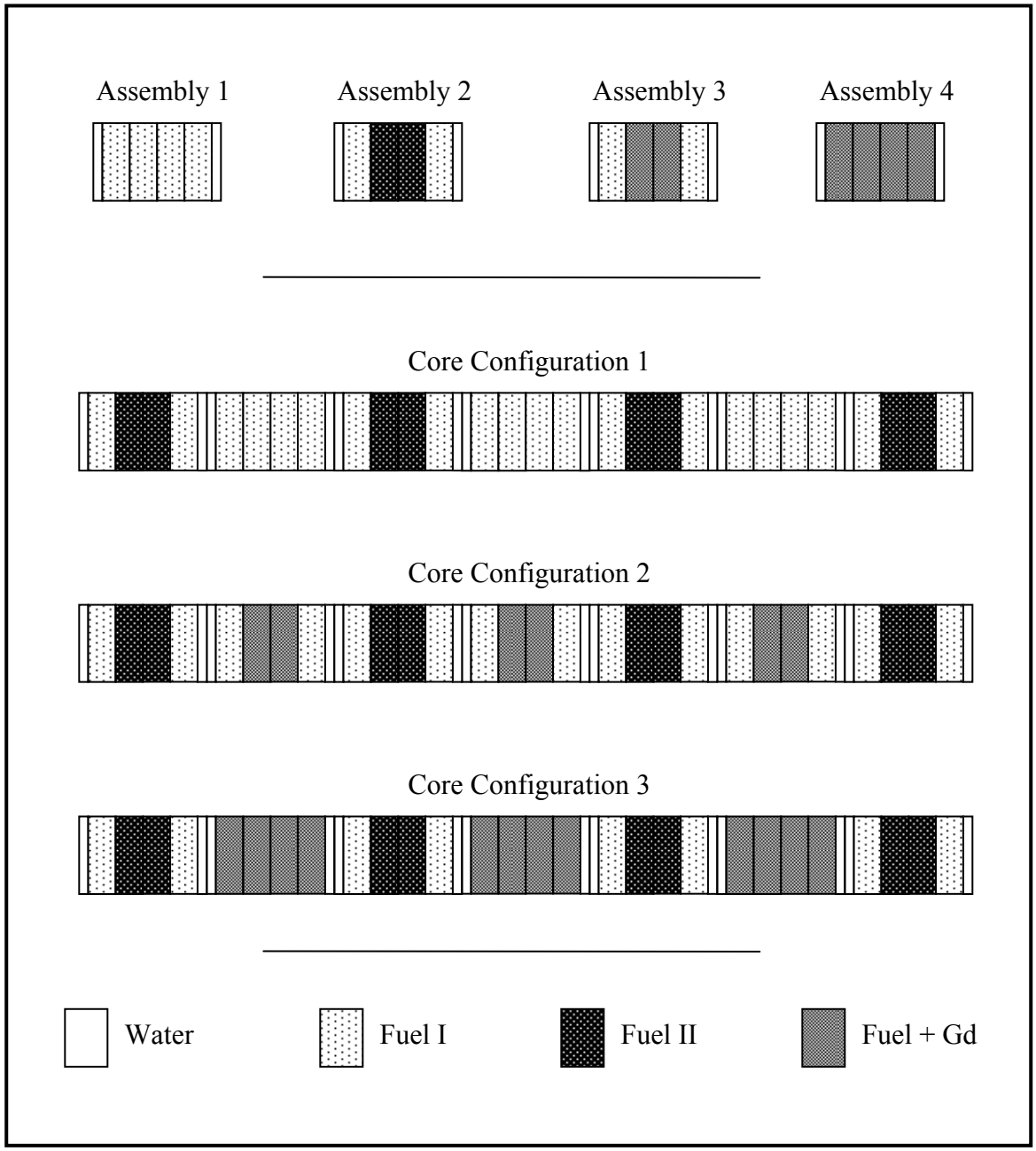

Figure 7: Assembly and Core Composition and Geometry

APPENDIX C
ERROR CALCULATIONS AND STATISTICS

All eigenvalue (k_{eff}) errors are expressed in mk (1 mk = 100 pcm = 10^{-3}) and computed by

$$\Delta k_{eff} = \left(k_{DIFFUSION} - k_{TRANSPORT}\right) \times 1000 . \tag{38}$$

Fission densities were computed on a per region basis. The fission density for region *i* is defined

$$f_i = \sum_{g=1}^{G} \sigma_{f,g}^{i} \hat{\varphi}_{i,g} \tag{39}$$

where G is the total number of groups and $\hat{\varphi}_{i,g}$ is the normalized flux in group g. When comparing a fission density value from a diffusion calculation, f_i^D, with a fission density value from a transport calculation, f_i^T, the relative error (or simply error) is computed by

$$e_i = \frac{f_i^D - f_i^T}{f_i^T} . \tag{40}$$

The following statistics are used to represent the set of errors from a specific calculation with I regions: average (AVG), root-mean-square average (RMS), mean relative error (MRE) and maximum (MAX). The definitions of these values follow:

$$AVG = \frac{1}{I} \sum_{i=1}^{I} \left| e_i \right| \tag{41}$$

$$RMS = \sqrt{\frac{1}{I} \sum_{i=1}^{I} e_i^2} \tag{42}$$

$$MRE = \frac{\sum_{i=1}^{I} f_i \left| e_i \right|}{\sum_{i=1}^{I} f_i} \tag{43}$$

$$MAX = \max_{1 \le i \le I} \left| e_i \right| . \tag{44}$$

REFERENCES

Bell, G. and Glasstone, S. *Nuclear Reactor Theory*, Robert E. Krieger Publishing Co., Huntington, NY (1979)

Briesmeister, J.F., "MCNP – A General Monte Carlo N-Particle Transport Code, Version 4C," Los Alamos National Laboratory, LA-13709-M (2000).

Brown, F. et al, "MCNP Version 5," *Transactions of the American Nuclear Society*, **87**, 273 (2003).

Casal, J.J., Stamm'ler, R.J.J., Villarino, E.A. and Ferri, A.A., "HELIOS: Geometric Capabilities of a New Fuel-Assembly Program," *Intl. Topical Meeting on Advances in Mathematics, Computations, and Reactor Physics*, Pittsburgh, Pennsylvania, April 28-May 2, **2**, 10.2.1, 1, (1991).

Ilas, D. and Rahnema, F., "A Heterogeneous Coarse Mesh Transport Method," *Transport Theory and Statistical Physics*, **32**(5-7), 445 (2003).

Ilas, G. and Rahnema, F., "A Monte Carlo Based Nodal Diffusion Model for Criticality Analysis of Spent Fuel Storage Lattices," Annals of Nuclear Energy, **30**(10), 1089 (2003).

Levermore, C. D. and Pomraning, G. C., "A flux-limited diffusion theory," *The Astrophysical Journal*, **248**, 321 (1981).

Olson, G. L., Auer, L. H. and Hall, M. L., "Diffusion, P_1, and other approximate forms of radiation transport," *Journal of Quantitative Spectroscopy and Radiative Transfer*, **64**, 619 (2000).

Pomraning, G. C., "Flux-Limited Diffusion Theory with Anisotropic Scattering," *Nuclear Science and Engineering*, **86**, 335 (1984).

Pounders, J., Rahnema, F. and Ilas, G. "CANDU Core Calculations with Monte Carlo Based Homogenized Cross Sections," *Transactions of the American Nuclear Society*, **92***,* 525, (2005).

Rahnema, F., Ilas, D. and Sitaraman, S., "Boiling Water Reactor Benchmark Calculations," *Nuclear Technology*, **117**(2), 184 (1997).

Redmond II, E. L., "Multigroup Cross Section Generation Via Monte Carlo Methods," PhD Thesis, Massachusetts Institute of Technology (1990).

Stamm'ler, R. J. J., *Methods of Steady-State Reactor Physics in Nuclear Design*, Academic Press Inc., London (1983).

Turinsky, F. et al, "NESTLE: A Few Group Neutron Diffusion Equation Solver Utilizing the Nodal Expansion Method (NEM) for Eigenvalue, Adjoint, and Fixed-Source Steady-State and Transient Problems," EGG-NRE-11406 (1994).

Turner, N. J. and Stone, J. M., "A Module for Radiation Hydrodynamic Calculations with ZEUS-2D Using Flux-limited Diffusion," *The Astrophysical Journal Supplement Series*, **135**, 95 (2001).